Therapeutic potential of extracellular vesicles derived from tetramethylpyrazine-preconditioned mesenchymal stem cells in a mouse model of aplastic anemia

LIXUAN CHEN[1*], PEINING DOU[2*], XIAOMIN ZHANG[3,4], FENGQI DUAN[5], LING KUI[6], XIAOYAN SUN[1], YANG XIAO[1,7], JIAN ZHANG[8] and ZENGHUI LIU[9]

[1]Department of Hematology, Shenzhen Qianhai Shekou Free Trade Zone Hospital, Shenzhen, Guangdong 518067, P.R. China; [2]First School of Clinical Medicine, Southern Medical University, Guangzhou, Guangdong 510515, P.R. China; [3]Department of Hematology and Oncology, Shenzhen University General Hospital, International Cancer Center, Hematology Institution, Haoshi Cell Therapy Institute of Shenzhen University, Shenzhen University Medical School, Shenzhen University, Shenzhen, Guangdong 518060, P.R. China; [4]Guangdong Key Laboratory for Biomedical Measurements and Ultrasound Imaging, National-Regional Key Technology Engineering Laboratory for Medical Ultrasound, School of Biomedical Engineering, Shenzhen University Medical School, Shenzhen, Guangdong 518060, P.R. China; [5]Department of Hematology, The Seventh Affiliated Hospital of Sun Yat-sen University, Sun Yat-sen University, Shenzhen, Guangdong 518106, P.R. China; [6]Department of Medical Laboratory, Shenzhen Qianhai Shekou Free Trade Zone Hospital, Shenzhen, Guangdong 518067, P.R. China; [7]Department of Hematology, Jiangmen Central Hospital, Jiangmen, Guangdong, Guangdong 529030, P.R. China; [8]Shenzhen Key Laboratory of Metabolic Health, Shenzhen Metabolism and Reproductive Targeted Delivery Proof-of-Concept Center, Shenzhen Institutes of Advanced Technology, Chinese Academy of Sciences, Shenzhen, Guangdong 518055, P.R. China; [9]Department of Hematology, The First Affiliated Hospital of Guangzhou University of Chinese Medicine, Guangzhou, Guangdong 510405, P.R. China

Received December 15, 2025; Accepted October 28, 2026

DOI: 10.3892/etm.2026.13358

Abstract. Acquired aplastic anemia (AA) is a severe hematological disorder characterized primarily by bone marrow (BM) failure and hypoplastic myelopoiesis. Extracellular vesicles (EVs) secreted by mesenchymal stem cells (MSCs) have emerged as a promising therapeutic approach for hematopoietic disorders. In the present study, MSCs-derived EVs were isolated by differential ultracentrifugation after *in vitro* stimulation of MSCs with tetramethylpyrazine (TMP); EV identity was verified by nanoparticle tracking analysis, transmission electron microscopy and western blotting for surface markers. An AA mouse model was subsequently established via cyclophosphamide combined with busulfan conditioning to evaluate the therapeutic effects of EVs on BM hematopoiesis. Western blotting was used to detect the expression of signaling-related proteins. Flow cytometry was performed to quantify T helper 17 (Th17) and regulatory T (Treg) cell proportions. The levels of hematopoietic cytokines were determined using an ELISA assay. And BM hematopoietic function was evaluated by blood cell counting and CD34 immunohistochemistry staining. TMP stimulation markedly increased EVs secretion into MSCs culture supernatants, potentially through the Rab27a/mammalian target of rapamycin complex 1 signaling axis. *In vivo*, EVs treatment significantly increased peripheral blood cell and BM nucleated cell counts, improved spleen indices and restored the disrupted Th17/Treg immune balance in AA mice. Moreover, EVs treatment effectively upregulated the expression of key hematopoietic regulators, including granulocyte-macrophage colony-stimulating factor, thrombopoietin and erythropoietin. In conclusion, the present findings support the potential

Correspondence to: Professor Jian Zhang, Shenzhen Key Laboratory of Metabolic Health, Shenzhen Metabolism and Reproductive Targeted Delivery Proof-of-Concept Center, Shenzhen Institutes of Advanced Technology, Chinese Academy of Sciences, 1068 Xueyuan Avenue, Shenzhen University Town, Xili, Nanshan, Shenzhen, Guangdong 518055, P.R. China
E-mail: jian.zhang@siat.ac.cn

Dr Zenghui Liu, Department of Hematology, The First Affiliated Hospital of Guangzhou University of Chinese Medicine, 16 Baiyun Airport Road, Baiyun, Guangzhou, Guangdong 510405, P.R. China
E-mail: 10304254@qq.com

*Contributed equally

Abbreviations: AA, aplastic anemia; MSCs, mesenchymal stem cells; EVs, extracellular vesicles; TMP, tetramethylpyrazine; BM, bone marrow; CM, conditioned medium; GM-CSF, granulocyte-macrophage colony stimulating factor; TPO, thrombopoietin; EPO, erythropoietin

Key words: mesenchymal stem cells, extracellular vesicles, tetramethylpyrazine, Rab27a/mTORC1, aplastic anemia

of MSC-derived EVs as a treatment for AA by improving hematopoietic function.

Introduction

Aplastic anemia (AA) is a refractory bone marrow (BM) failure disorder characterized by myeloid hypoplasia, pancytopenia and associated clinical manifestations, including anemia, hemorrhage and infection (1,2). Immunosuppressive therapy and allogeneic hematopoietic stem cell transplantation are currently the standard first-line treatments for AA (3). However, their clinical application is substantially limited by several factors, including disease severity, patient age, treatment-related cytotoxicity, donor scarcity and the high risk of graft-versus-host disease (4,5).

Mesenchymal stem cells (MSCs) have emerged as promising therapeutic candidates for various refractory diseases because of their immunomodulatory, hematopoietic-supportive, proangiogenic and regenerative properties. Accumulating clinical evidence indicates that MSC transplantation promotes hematopoietic recovery and restores immune homeostasis in patients with AA (6-8). Consistent with these findings, our previous clinical data showed that 33.3% of patients with AA achieved complete or partial remission after MSCs transplantation (9). Despite the well-documented therapeutic potential of MSCs, conventional MSCs-based therapy has several unavoidable limitations, including inconsistent cell quality, poor survival of transplanted cells, donor age-related functional heterogeneity, ectopic differentiation and a potential risk of tumorigenesis (10-12).

Given the limitations of cell-based therapies, MSCs-derived extracellular vesicles (MSCs-EVs) have attracted considerable attention as a novel cell-free therapeutic alternative. EVs are lipid bilayer-enclosed vesicles secreted by various cell types and contain abundant bioactive molecules, including noncoding RNAs, genomic DNA, lipids and growth factors (13,14). Growing evidence indicates that MSCs-EVs exert regenerative and anti-inflammatory effects in multiple disease models (15-17). Nevertheless, the clinical translation of MSCs-EVs is substantially hindered by their insufficient yield, low purity and inherent heterogeneity. Improving the production efficiency and quality of EVs has therefore become an important priority for their clinical application.

Tetramethylpyrazine (TMP), a major bioactive alkaloid derived from the traditional Chinese medicinal herb Ligusticum chuanxiong Hort., has been shown to regulate cellular EVs secretion and alter EVs cargo composition (18-20). Studies have also demonstrated that TMP delays MSCs senescence, enhances MSCs self-renewal and improves the therapeutic efficacy of MSCs in models of autoimmune encephalomyelitis (21,22). However, the therapeutic efficacy and underlying molecular mechanisms of EVs derived from TMP-preconditioned MSCs in AA remain poorly understood. The present study aimed to explore whether TMP promotes EV secretion from MSCs through the Rab27a/mammalian target of rapamycin complex 1 (mTORC1) signaling pathway; and compare the therapeutic effects of negative control (NC)-EVs and TMP-EVs on BM hematopoietic function and T helper 17 (Th17)/regulatory T cell (Treg) immune homeostasis in an AA mouse model. In the present study, EVs were isolated from untreated MSCs (NC-EVs) and TMP-preconditioned MSCs (TMP-EVs) and their protective effects on BM hematopoiesis were systematically evaluated in a mouse model of AA. The regulatory effects of TMP on MSCs was also investigated and Rab27a and mTORC1 expression was assessed to explore the potential molecular mechanisms underlying TMP-mediated EVs secretion.

Materials and methods

Isolation, culture and treatment of human umbilical cord-derived MSCs

Isolation of MSCs from human umbilical cords. Human umbilical cords were provided by Shenzhen Wingor Biotechnology Co., Ltd. and obtained from full-term infants delivered by cesarean section after uncomplicated pregnancies. Human umbilical cords were donated by 6 healthy pregnant women (all female; median age 30 years, range 26-35 years), and the corresponding neonates comprised 3 males and 3 females. Written informed consent was obtained from all donors. Briefly, the umbilical cord tissues were thoroughly rinsed, and Wharton's jelly was isolated and cut into small fragments (1-2 mm^3). The minced tissue fragments were evenly seeded into culture flasks and maintained in human MSCs serum-free medium (cat. no. SC2013-G-A; Tianjin Haoyang Huahai Biotechnology Co., Ltd.) containing 10% human MSCs serum-free basic medium addition (cat. no. SC2013-G-B; Tianjin Haoyang Huahai Biotechnology Co., Ltd.) for 14 days. When the adherent cells reached ~80% confluence, the tissue fragments were removed, and the cells were collected for subsequent passaging. Passage 3 MSCs were used for all experiments. The surface marker profiles of the MSCs were characterized by flow cytometry using the following primary antibodies from BioLegend, Inc.: Anti-human CD45 (cat. no. 304012), anti-human CD34 (cat. no. 343612), anti-human CD73 (cat. no. 344015, anti-human CD90 (cat. no. 328106), anti-human CD105 (cat. no. 323219), anti-human CD11b (cat. no. 301304) and anti-human HLA-DR (cat. no. 361609).

Cells culture and experimental treatment of MSCs. Passage 3 MSCs were cultured in serum-free human MSCs medium (cat. no. SC2013-G-A; Tianjin Haoyang Huahai Biotechnology Co., Ltd.) supplemented with 10% serum-free human MSCs medium additive (cat. no. SC2013-G-B; Tianjin Haoyang Huahai Biotechnology Co., Ltd.). The cells were incubated at 37˚C in a humidified atmosphere containing 5% CO_2. To optimize EVs secretion, MSCs were treated with different concentrations of TMP (cat. no. 1124-11-4; Shanghai Macklin Biochemical Co., Ltd.). Specifically, MSCs were seeded in 96-well plates at $3x10^3$ cells per well or culture dishes at $2x10^4$ cells/cm^2. After complete adherence, the cells were continuously exposed to TMP at concentrations of 10, 20 or 30 μg/ml at 37˚C with 95% humidity and 5% CO_2 for 48 h. Cell viability and proliferation were subsequently assessed using a CCK-8 kit (cat. no. CK04; Dojindo Laboratories, Inc.) in accordance with the manufacturer's instructions.

Detection of Rab27a and mTORC1 expression by western blot. Total cellular protein was extracted from MSCs using RIPA lysis buffer (cat. no. P0013B; Beyotime Biotechnology) supplemented with a protease inhibitor cocktail (cat. no. P1008;

Beyotime Biotechnology). Protein concentrations were determined using a BCA protein assay kit (cat. no. 23227; Thermo Fisher Scientific, Inc.). A total of 30 μg of protein from each sample was separated using a 4-12% gradient SDS-PAGE gel and transferred onto polyvinylidene fluoride membranes (cat. no. IPVH00010; MilliporeSigma). After blocking with 5% skim milk for 1 h at room temperature, the membranes were incubated overnight at 4˚C with primary antibodies against Rab27a (1:1,000; cat. no. ab103418; Abcam), mTORC1 (1:5,000; cat. no. ab134903; Abcam) and GAPDH (1:1,000; cat. no. AF0006; Beyotime Biotechnology). The following day, the membranes were thoroughly washed and incubated with horseradish peroxidase-conjugated secondary antibodies (1:1,000; cat. no. A0208; Beyotime Biotechnology) for 1 h at room temperature. Protein bands were visualized using an enhanced chemiluminescence reagent (cat. no. BMU102; Abbkine Scientific Co., Ltd.) and captured with a Bio-Rad ChemiDoc XRS system (Bio-Rad Laboratories, Inc.). The relative expression levels of Rab27a and mTORC1 were quantified using ImageQuant LAS 4000 software (Cytiva).

Isolation and characterization of EVs

Isolation and purification of EVs. EVs were isolated from the conditioned medium of untreated MSCs (NC-EVs) and TMP-preconditioned MSCs (TMP-EVs) using a sequential centrifugation protocol with a Beckman Optima XPN ultracentrifuge (Beckman Coulter, Inc.). Briefly, the collected conditioned medium was initially centrifuged at 600 x g for 10 min at 4˚C to remove intact cells. The supernatant was then centrifuged at 2,000 x g for 10 min at 4˚C to remove dead cells and cell fragments, followed by centrifugation at 10,000 x g for 30 min at 4˚C to eliminate cellular debris. The clarified supernatant was subsequently ultracentrifuged at 100,000 x g for 70 min at 4˚C to pellet crude EVs. The resulting pellet was resuspended in sterile phosphate-buffered saline (PBS) and subjected to a second ultracentrifugation step under the same conditions for further purification. The purified NC-EVs and TMP-EVs were collected separately and stored at -80˚C until further use.

Biological characterization of EVs. Western blot analysis was performed to detect EVs-specific protein markers. EVs samples were lysed using RIPA lysis buffer (cat. no. P0013B; Beyotime Biotechnology), and total protein concentrations were determined using a BCA protein assay kit (cat. no. 23227; Thermo Fisher Scientific, Inc.). A total of 30 μg of protein per lane was separated by 12% SDS-PAGE and transferred onto polyvinylidene fluoride membranes (cat. no. IPVH00010; MilliporeSigma). After blocking with 5% skim milk at room temperature for 1 h, the membranes were incubated with primary antibodies against CD9 (1:1,500; cat. no. MA5-31980; Thermo Fisher Scientific, Inc.) and CD63 (1:2,000; cat. no. 10628D; Thermo Fisher Scientific, Inc.) at 4˚C overnight, followed by incubation with horseradish peroxidase-conjugated secondary antibodies at room temperature for 1 h. Protein bands were visualized and analyzed using a Bio-Rad ChemiDoc XRS imaging system.

The particle concentration and size distribution of the EVs were determined by nanoparticle tracking analysis (NTA; NanoSight NS300, Malvern Panalytical Ltd.). Briefly, the EVs samples were appropriately diluted with sterile PBS to a final volume of 1 ml and transferred into a quartz cuvette. All samples were analyzed at 25˚C in accordance with the standard operating procedures of the instrument. Particle characterization reports were automatically generated and analyzed after data acquisition.

Transmission electron microscopy (TEM) was used to examine EVs morphology. Briefly, 10 μl of the EVs suspension was diluted with an equal volume of PBS. The diluted sample was placed onto a 300-mesh carbon-Formvar-coated copper grid and incubated for 2 min at room temperature. After excess liquid was removed, the samples were negatively stained with 3% (w/v) sodium phosphotungstate solution for 5 min at room temperature. The grids were then gently rinsed with distilled water and air-dried at room temperature. EVs morphology was examined and imaged using a JEM-1400 transmission electron microscope (JEOL, Ltd.) at an accelerating voltage of 80 kV.

Establishment of AA mouse model and experimental design. Healthy male ICR mice (8 weeks old; body weight, 20±2 g) were purchased from the Experimental Animal Center of Southern Medical University (Guangzhou, China). All mice were housed under standard controlled conditions at a constant temperature of 22±2˚C, a relative humidity of 50±10% and a 12-h light/dark cycle. All animal experiments were conducted at the Experimental Animal Center of Southern Medical University. All procedures were approved by the Institutional Animal Care and Use Committee of Southern Medical University (approval no. SMUL2022228) and performed in accordance with the ARRIVE guidelines.

To establish the murine AA model, mice received intraperitoneal injections of busulfan (20 mg/kg; CAS no. 55-98-1; Shanghai Macklin Biochemical Co., Ltd.) and cyclophosphamide (80 mg/kg; CAS no. 6055-19-2; MilliporeSigma) once daily for 7 consecutive days. Age-matched healthy control mice were injected with an equal volume of sterile PBS. On day 8 after model induction, the AA mice were randomly assigned to the intervention groups. EVs samples were resuspended in 100 μl of sterile PBS and administered via tail vein injection. The animals were divided into four groups (n=8 per group): Blank control group (healthy mice treated with PBS), AA model group (model mice treated with PBS), NC-EVs group (AA mice treated with 100 μg of EVs derived from untreated MSCs) and TMP-EVs group (AA mice treated with 100 μg of EVs derived from TMP-preconditioned MSCs).

Peripheral blood cell counts and hematopoietic factors detection. On day 15 after treatment, peripheral blood samples were collected from the orbital venous plexus to evaluate pancytopenia. Blood cell counts were determined using a veterinary hematology analyzer (Mindray BC-30 Vet). Serum samples were prepared according to standard procedures for the measurement of hematopoietic cytokines. Briefly, whole-blood samples were maintained at room temperature for at least 1 h and then centrifuged at 2,000 x g for 10 min at room temperature. The serum supernatant was collected for subsequent analysis. Serum levels of granulocyte-macrophage colony-stimulating factor (GM-CSF), thrombopoietin (TPO) and erythropoietin (EPO) were quantified using commercial ELISA kits (cat. nos. MM-0185M1, MM-0130M1 and MM-0194M1, respectively; Jiangsu Meimian Industrial Co., Ltd., China) according to the manufacturer's instructions.

Detection of immune organs index and T lymphocyte subsets

Measurement of spleen and thymus indices. After blood collection, all mice were humanely euthanized by carbon dioxide inhalation. CO_2 gas was supplied to the chamber at a volume displacement rate of 50% of the chamber volume per minute. The spleen and thymus were rapidly excised, and the surrounding adipose tissue was removed. Residual blood on the organ surfaces was absorbed using filter paper. The wet weight of each organ was measured using a high-precision electronic balance. The spleen and thymus indices were calculated as the ratio of the respective organ weight to body weight.

Detection of Th17 and Treg cells proportion. Flow cytometry was used to determine the proportions of Th17 and Treg cells among peripheral blood mononuclear cells. Cell staining was performed using a Mouse Th17 Staining Kit (cat. no. KTH217; Multi Sciences Biotech) and a Mouse Regulatory T Cell Staining Kit (cat. no. KTR201; Multi Sciences Biotech). Briefly, the isolated cells were first stained with surface antibodies against CD3, CD4 and CD25 for 15 min at room temperature in the dark. And the intracellular staining for Foxp3 and IL-17A was performed for 30 min at room temperature in the dark. The stained cells were analyzed by FACSVerse flow cytometry (BD Biosciences), and the proportions of the target cell populations within the designated gates were quantified using FlowJo software (v10.8.1; BD Biosciences).

Histopathological evaluation and cytological analysis of BM

Histological examination and counting of BM nucleated cells. On day 15 after treatment, the mice were euthanized, and the femurs were harvested. The left femurs were fixed, decalcified, embedded in paraffin, serially sectioned and the sections were stained with hematoxylin for 5 min at room temperature, followed by eosin staining for 1 min at room temperature. Morphological changes and hematopoietic status in the BM were examined and imaged under a light microscope. BM cells were simultaneously flushed from the right femurs with sterile PBS to prepare single-cell suspensions. The number of BM nucleated cells was determined using a hematology analyzer.

CD34 immunohistochemistry staining. To further evaluate BM hematopoietic function in mice, CD34+ cells were detected by immunohistochemistry. After deparaffinization and rehydration, the BM sections were treated with 3% hydrogen peroxide for 10 min at room temperature to block endogenous peroxidase activity. The sections were then washed and heated in 10 mM citrate buffer (pH 6.0) for 15 min for antigen retrieval. Subsequently, the sections were blocked with 3% normal goat serum (cat. no. G1208; Servicebio Biotechnology Co., Ltd.) for 60 min at room temperature and incubated overnight at 4˚C with an anti-CD34 antibody (1:500; cat. no. ET1606-11; HUABIO). After washing, the sections were incubated with the secondary antibody for 30 min at room temperature. Immunoreactivity was visualized using a DAB staining kit (cat. no. P0202; Beyotime Biotechnology) according to the manufacturer's instructions. The sections were then counterstained with hematoxylin for 3 min at room temperature, dehydrated and coverslipped. For each animal, 4 non-overlapping sections were examined using an upright light microscope (Olympus BX53; Olympus Corporation), and 5 random high-power fields (magnification, x200) were imaged per section, excluding necrotic regions. Image analysis was performed in ImageJ v1.54f (National Institutes of Health) by an investigator blinded to group information. The area fraction of CD34-positive staining was quantified in ImageJ. After color deconvolution to separate DAB signal from hematoxylin counterstain, a fixed threshold was applied to segment DAB-positive regions. The CD34-positive area fraction was calculated as the ratio of positive stained area to the total tissue area within each field. The average positive area fraction per animal was used for statistical comparison.

Biosafety and toxicity evaluation of EVs. To evaluate the safety of MSCs-EVs in mice, the major internal organs, including the heart, lungs, liver, kidneys and spleen, were examined macroscopically. Tissue samples were collected for routine histopathological examination and hematoxylin and eosin staining using the same procedures described for the BM samples. Blood samples were collected for biochemical parameters detection, including alanine aminotransferase, aspartate aminotransferase and creatinine, were also measured. All analyses were performed using a ChemWell 2310 automated biochemical analyzer (Awareness Technology, Inc.), the corresponding reagents, and GBG ChemWell® software v2.7 (Awareness Technology, Inc.) in accordance with the manufacturer's instructions.

Statistical analysis. All statistical analyses were performed using Stata version 13.0 (StataCorp LP). All experiments were independently repeated three times. Quantitative data are presented as the mean ± standard error. One-way analysis of variance (ANOVA) was used for comparisons among multiple groups, followed by Bonferroni-corrected pairwise post hoc comparisons. Data with skewed distributions or unequal variances were analyzed using the Kruskal-Wallis H test, followed by Dunn's multiple comparison test. $P<0.05$ was considered to indicate a statistically significant difference.

Results

TMP promotes EVs secretion of MSCs by regulating Rab27a/mTORC1. Firstly, the surface marker profiles of MSCs isolated from human umbilical cords were assessed by flow cytometry. The isolated and cultured cells showed high expression of CD73, CD90 and CD105 but were negative for CD34, CD45, CD11b and HLA-DR, consistent with the typical characteristics of MSCs (23) (Fig. 1A). To determine a safe and effective concentration of TMP for MSCs treatment, the effects of TMP on MSCs viability and EVs secretion was assessed. Cell viability assays showed that TMP concentrations ranging from 0 to 20 μg/ml had no apparent cytotoxic effects on MSCs. By contrast, treatment with 30 μg/ml TMP significantly reduced MSCs viability ($P<0.05$), indicating that high-dose TMP was cytotoxic to MSCs (Fig. 1B).

NTA revealed that TMP treatment markedly increased the number of EVs particles secreted by MSCs compared with the control group, with the greatest increase observed in the 30 μg/ml group ($P<0.05$; Fig. 1C). Western blot analysis further

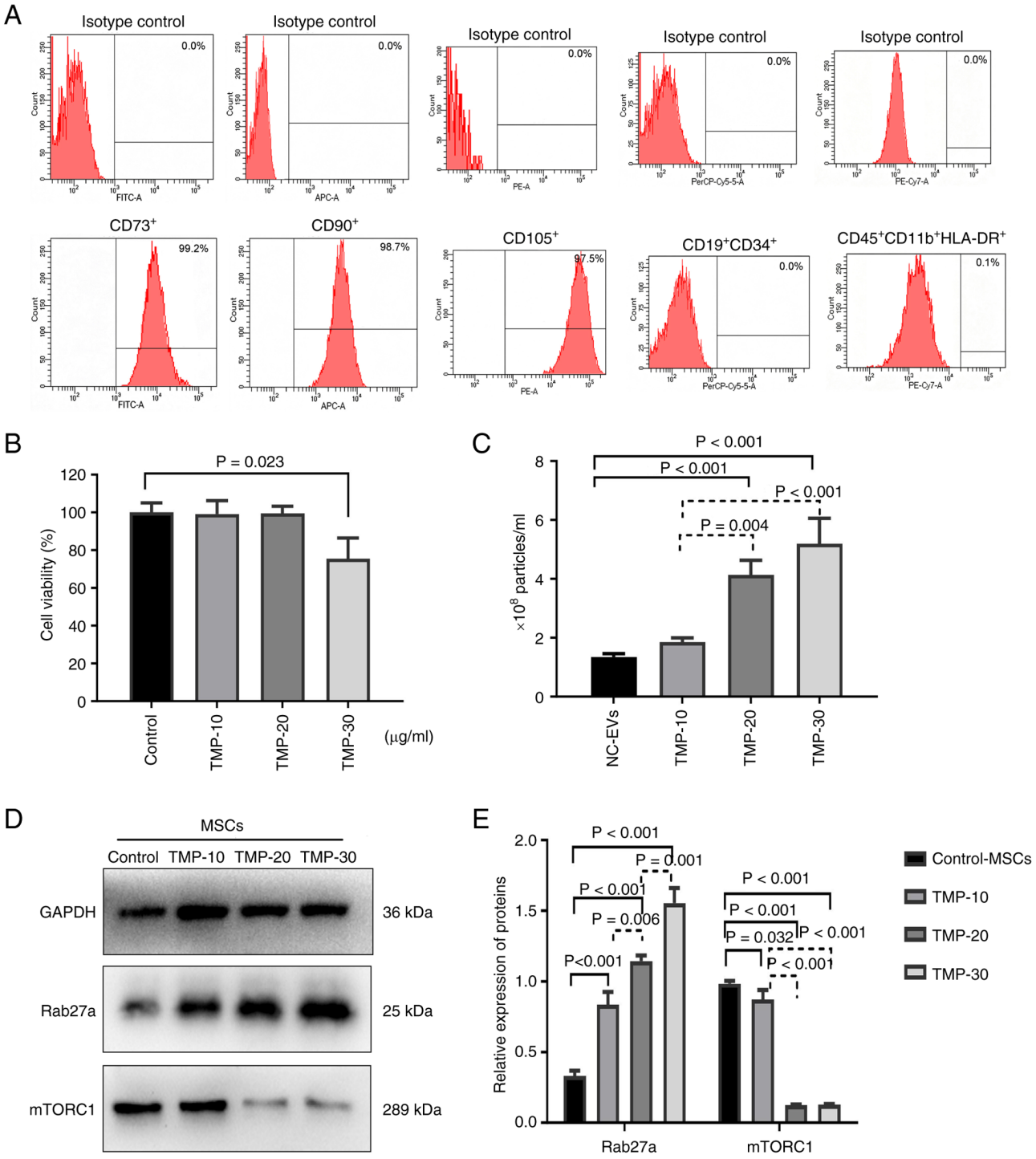


Figure 1. Effects of TMP on cell viability and extracellular vesicles secretion of MSCs. Data are presented as mean ± SD; n=3 per group. Statistical analysis was performed using one-way ANOVA followed by Bonferroni comparison test. (A) Representative flow cytometric histograms showing the expression of MSCs surface markers. Isotype controls were used to define the positive threshold, with identical gating applied to paired MSCs samples. MSCs were positive for CD73, CD90 and CD105, and negative for CD19, CD34, CD45, CD11b and HLA-DR. (B) The cell viability of MSCs after TMP treatment. (C) Number of particles of EVs from MSCs. (D) The protein expression of Rab27a and mTORC1 in MSCs after TMP treatment. (E) Statistical diagram of relative expression levels of Rab27a and mTORC1 proteins. TMP, tetramethylpyrazine; MSCs, mesenchymal stem cells; EVs, extracellular vesicles.

confirmed that TMP promoted EVs secretion. Specifically, treatment with 10 or 20 μg/ml TMP significantly increased the level of the EVs-specific marker CD9 in MSCs-derived EVs, whereas treatment with 20 or 30 μg/ml TMP increased CD63 protein levels (Fig. 2A). When considered together with the cell viability results, 20 μg/ml TMP exerted the strongest stimulatory effect on EVs secretion without inducing cytotoxicity. Therefore, 20 μg/ml was selected as the optimal TMP concentration for subsequent experiments.

To investigate the potential molecular mechanisms underlying TMP-induced EVs secretion, the expression of Rab27a and mTORC1, two key regulators of EVs biogenesis and secretion, were examined. TMP treatment significantly increased Rab27a expression and decreased mTORC1 expression in

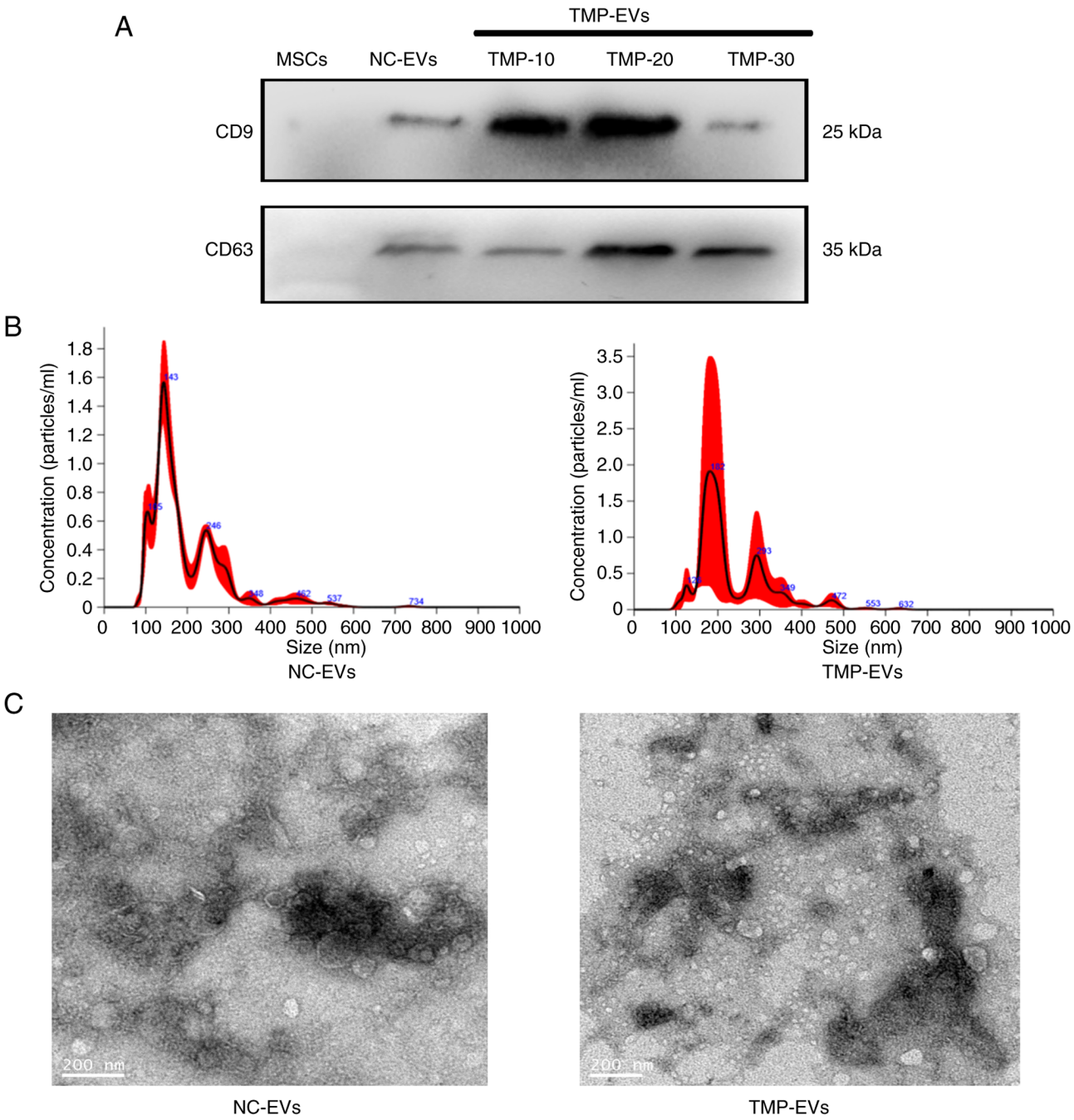


Figure 2. Characterization of EVs. Data are presented as mean ± SD. n=3 per group. Statistical analysis was performed using one-way ANOVA followed by Bonferroni comparison test. (A) The protein expression of CD63 and CD9 of EVs. (B) The concentration and particle size distribution of the EVs was determined by nanoparticle tracking analysis. (C) The morphology of EVs was observed by transmission electron microscopy. EVs, extracellular vesicles; TMP, tetramethylpyrazine; MSCs, mesenchymal stem cells; NC-EVs, untreated EVs.

MSCs ($P<0.05$; Fig. 1D and E). These findings suggest that TMP-induced EVs secretion may be associated with Rab27a upregulation and mTORC1 downregulation.

Identification and characterization of EVs. To confirm the successful isolation and purification of MSCs-derived EVs, their biological characteristics were systematically evaluated by western blotting, NTA and TEM. Western blot confirmed the expression of the canonical EV markers CD9 and CD63 in both purified EVs preparations (Fig. 2A), consistent with the molecular characteristics of EVs (24).

NTA showed that the isolated vesicles exhibited a relatively homogeneous size distribution, with diameters predominantly ranging from 40 to 200 nm, within the typical size range of EVs (Fig. 2B). TEM further confirmed the intact morphology of the isolated vesicles, which displayed regular round or spherical structures (Fig. 2C). Collectively, the marker expression, particle size distribution and morphological characteristics confirmed the successful isolation of EVs derived from untreated MSCs (NC-EVs) and TMP-preconditioned MSCs (TMP-EVs) with structural integrity.

Table I. Blood biochemical assays.

Parameter	Blank	AA model	NC-EVs	TMP-EVs	P-value
ALT, U/l	95.15±6.73	89.14±9.33	90.37±6.93	88.45±10.22	P>0.05
AST, U/l	121.18±10.65	118.59±9.73	120.68±7.95	127.68±5.72	
CREA-S, μmol/l (mol/ml)	31.21±10.24	29.78±6.87	35.42±8.34	31.55±6.45	

Data are presented as the mean ± SD; n=6. Statistical comparison compared with the blank control. ALT. alanine aminotransferase; AST, aspartate aminotransferase; CREA-S, creatinine; EVs, extracellular vesicles; TMP, tetramethylpyrazine; NC-EVs, untreated EVs; AA, aplastic anemia.

Therapeutic effect of EVs on hematopoietic dysfunction in AA mice. A mouse model of AA was established to evaluate the therapeutic effects of EVs on AA-associated hematopoietic dysfunction. Routine peripheral blood analysis showed that, compared with healthy control mice, AA model mice had significantly lower white blood cell (WBC), red blood cell (RBC), and platelet (PLT) counts and reduced hemoglobin (Hb) levels (P<0.05; Fig. 3A), recapitulating the characteristic pancytopenic phenotype of clinical AA. Treatment with either NC-EVs or TMP-EVs significantly alleviated peripheral cytopenia and restored WBC, RBC and PLT counts and Hb levels in AA mice (P<0.05; Fig. 3A). Notably, TMP-EVs produced a greater increase in WBC counts, whereas no significant differences were observed between the NC-EVs and TMP-EVs groups in the other hematological parameters (P>0.05).

Quantification of BM nucleated cells and immunohistochemical staining for CD34+ hematopoietic stem/progenitor cells revealed marked reductions in BM nucleated cell counts and CD34+ in AA model mice (Fig. 3C-E), indicating severe BM hematopoietic failure. EVs treatment substantially increased the number of BM nucleated cells and the proportion of CD34+ cells in AA mice, with the highest CD34 positivity observed in the TMP-EVs group (P<0.05; Fig. 3E).

BM histopathological examination further supported the therapeutic effects of EVs. The BM of AA model mice exhibited reduced hematopoietic cellularity and extensive adipose infiltration, indicating impaired hematopoietic recovery. Following treatment with NC-EVs or TMP-EVs, hematopoietic cell density was markedly increased, whereas adipose tissue hyperplasia was attenuated (Fig. 3B). These results indicate that MSCs-derived EVs alleviate BM hematopoietic dysfunction and promote hematopoietic recovery in AA mice.

Regulatory effect of EVs on hematopoietic cytokines in AA mice. To further investigate the mechanisms by which EVs improve hematopoietic function, the levels of key hematopoietic regulatory cytokines were measured in the BM of mice. Compared with healthy mice, AA model mice exhibited markedly lower levels of GM-CSF, EPO and TPO (P<0.01; Fig. 3F), which may contribute to impaired BM hematopoiesis. Treatment with either NC-EVs or TMP-EVs significantly restored GM-CSF, EPO and TPO levels in AA mice (P<0.05; Fig. 3F). No significant differences in the regulation of these hematopoietic cytokines were observed between the two EVs treatment groups.

Immunomodulatory effect of EVs on AA mice. The pathogenesis of AA is closely associated with immune dysregulation. The immunomodulatory effects of EVs in AA mice were therefore evaluated by assessing immune organ indices and the proportions of peripheral T-lymphocyte subsets. AA model mice exhibited significantly lower spleen and thymus indices than healthy mice, suggesting immune organ atrophy and impaired immune function. EVs treatment significantly restored the spleen index in AA mice (P<0.05; Fig. 4C), whereas no significant change was observed in the thymus index, indicating that EVs partially ameliorated immune organ damage in AA mice.

Flow cytometric analysis of peripheral blood T-lymphocyte subsets revealed a marked immune imbalance in AA model mice, characterized by an increased proportion of Th17 cells and a reduced proportion of Treg cells. Treatment with NC-EVs or TMP-EVs significantly reduced the proportion of Th17 cells and increased the proportion of Treg cells (P<0.05; Fig. 4A and B), with TMP-EVs producing a more pronounced immunomodulatory effect. These findings indicate that EVs restore the Th17/Treg balance and improve the dysregulated immune microenvironment, thereby potentially facilitating BM hematopoietic recovery in AA mice.

In vivo biosafety evaluation of MSCs-derived EVs. To evaluate the *in vivo* biosafety of systemically administered MSCs-derived EVs, the histopathological features of major organs were examined and peripheral blood biochemical parameters were measured in experimental mice. Histopathological examination revealed no notable inflammatory infiltration, tissue necrosis or other pathological lesions in the heart, liver, spleen, lungs or kidneys after repeated intravenous administration of EVs (Fig. 4D).

Consistent with the histological findings, blood biochemical analyses showed that the levels of the liver function markers alanine aminotransferase and aspartate aminotransferase, as well as the renal function marker creatinine, remained unchanged in EVs-treated mice compared with control mice, with no evidence of hepatic or renal toxicity (Table I). These findings indicate that repeated intravenous administration of MSCs-derived EVs was well tolerated *in vivo* and did not induce detectable pathological changes or biochemical abnormalities in major organs.

Discussion

AA is a severe hematopoietic failure disorder with a complex etiology and pathogenesis, characterized primarily by

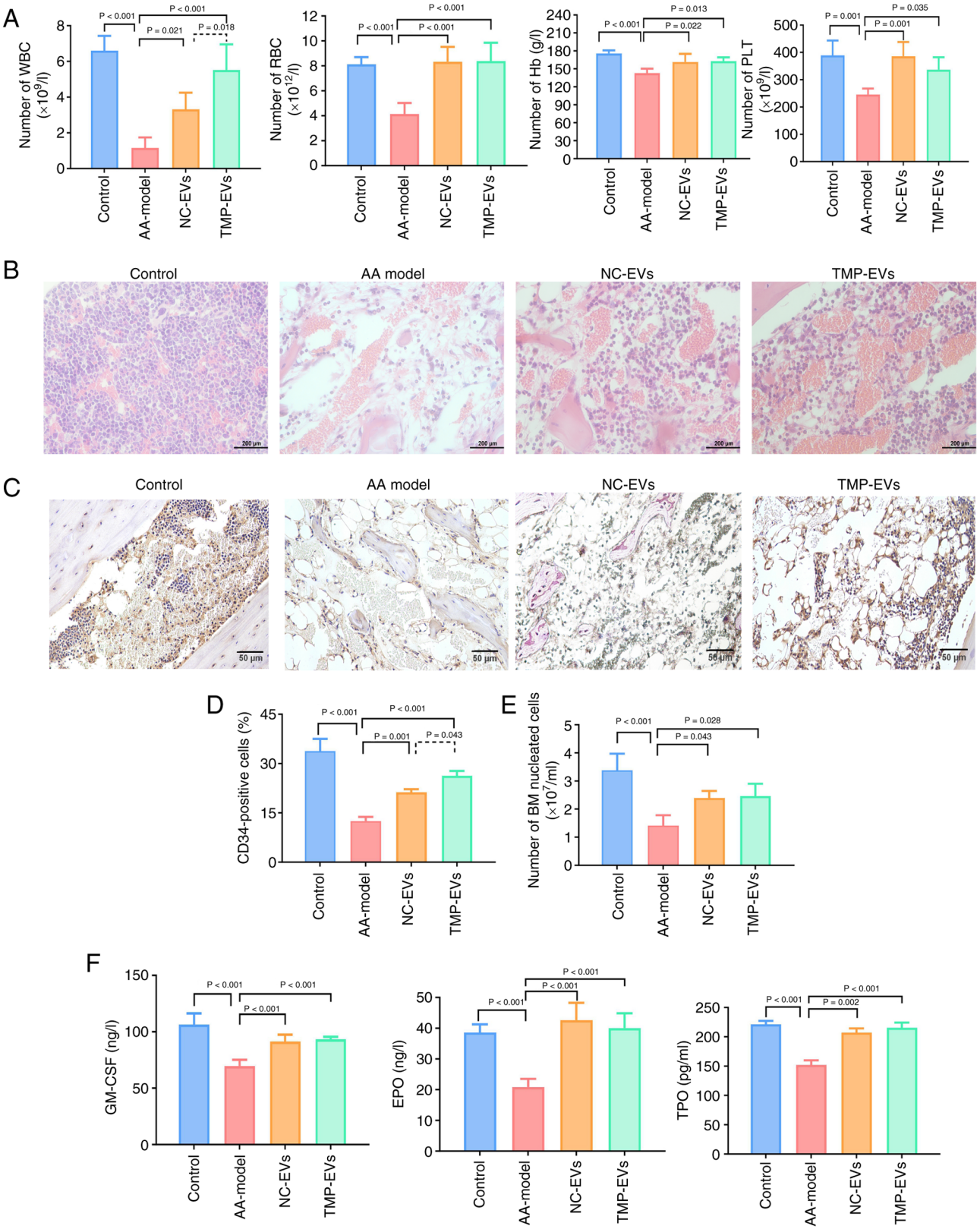


Figure 3. Effects EVs on the hematopoietic function in mice. Data are presented as mean ± SD. n=8 per group. Statistical analysis was performed using one-way ANOVA followed by Bonferroni comparison test. (A) The number of peripheral blood cells in mice. (B) The histological examination of BM in mice. (C) The immunohistochemical staining of CD34+ cells in bone marrow. (D) Statistical diagram of immunohistochemical staining of CD34+ cells. (E) The number of nucleated cells. (F) The levels of GM-CSF, EPO and TPO. EVs, extracellular vesicles; TMP, tetramethylpyrazine; MSCs, mesenchymal stem cells; NC-EVs, untreated EVs; BM, bone marrow; GM-CSF, granulocyte-macrophage colony stimulating factor; TPO, thrombopoietin; EPO, erythropoietin.

hematopoietic stem cell impairment, disruption of the BM microenvironment and immune dysregulation (25). MSCs contribute to tissue repair, immune regulation and metabolic homeostasis predominantly through paracrine activity, which

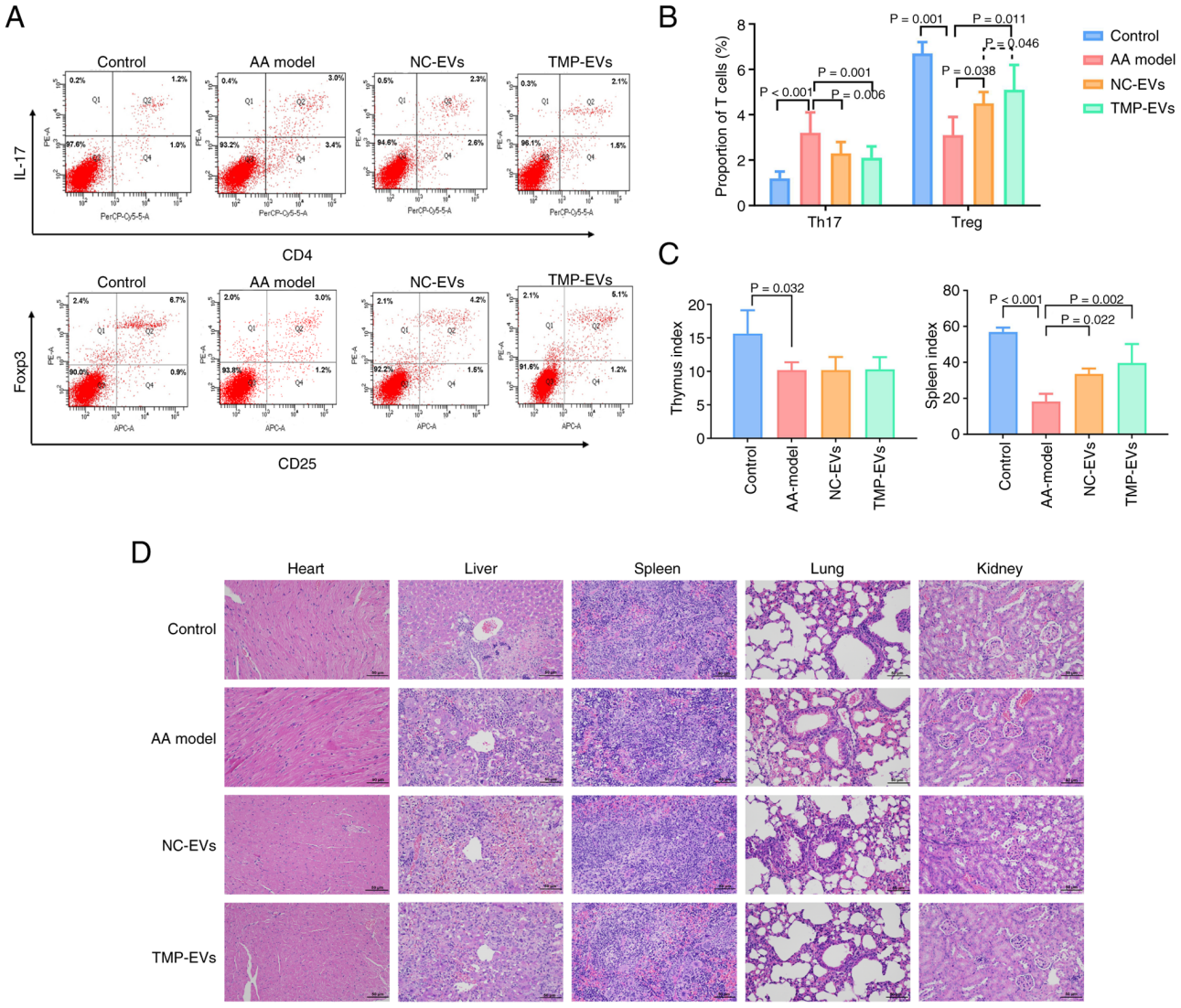


Figure 4. Immunomodulatory effect and biosafety evaluation of EVs on AA mice. Data are presented as mean ± SD. n=4 per group. Statistical analysis was performed using one-way ANOVA followed by Bonferroni comparison test. (A) The proportion of Th17 and Treg cells in mice analyzed by flow cytometry. (B) Quantitative analysis of the proportion of Th17 and Treg cells. (C) The spleen index and thymus index in mice. (D) The histopathological morphology of major visceral organs. EVs, extracellular vesicles; TMP, tetramethylpyrazine; MSCs, mesenchymal stem cells; NC-EVs, untreated EVs; Th17, T helper 17 cells; Tregs, regulatory T cells.

may be more biologically relevant than their differentiation capacity (26). EVs, as major paracrine products of MSCs, retain many of the functional properties of their parental cells and have emerged as promising cell-free alternatives to conventional cell therapy (27). However, the large-scale production and efficient isolation of EVs remain substantial barriers to their clinical application.

In recent years, numerous studies have sought to increase EVs yield by optimizing cell culture systems and isolation methods. Representative strategies include the use of three-dimensional culture systems to enhance cellular secretory capacity (28,29) and advanced ultrafiltration-based isolation protocols (30,31). Accumulating evidence also supports a role for TMP in regulating EVs secretion. Ruan *et al* (18) demonstrated that TMP treatment effectively increased EVs release from MSCs. Similarly, EVs secreted by MSCs treated with Suxiao Jiuxin Pill, a compound preparation containing TMP as a major component, promoted cardiomyocyte proliferation (19). TMP-preconditioned MSCs-EVs have also been reported to exert neuroprotective effects and promote axonal plasticity (20). Our previous study further showed that TMP ameliorated BM injury by regulating apoptotic signaling pathways in mice with BM failure (32). Nevertheless, the therapeutic effects of TMP-modified EVs in AA remain unclear. In the present study, TMP was used to stimulate EVs secretion from MSCs, and the therapeutic effects of TMP-induced EVs were systematically evaluated in a mouse model of AA. Both NC-EVs and TMP-EVs significantly increased peripheral WBC and PLT counts and the number of BM nucleated cells in AA mice. In addition, EVs treatment substantially increased the number of BM nucleated cells and the proportion of CD34+ cells in AA mice, with the highest CD34 positivity observed in the TMP-EVs group. The levels of key hematopoietic factors, including EPO, TPO and GM-CSF, were also markedly increased after EVs treatment. These results indicate that EV can effectively improve the hematopoietic function of AA

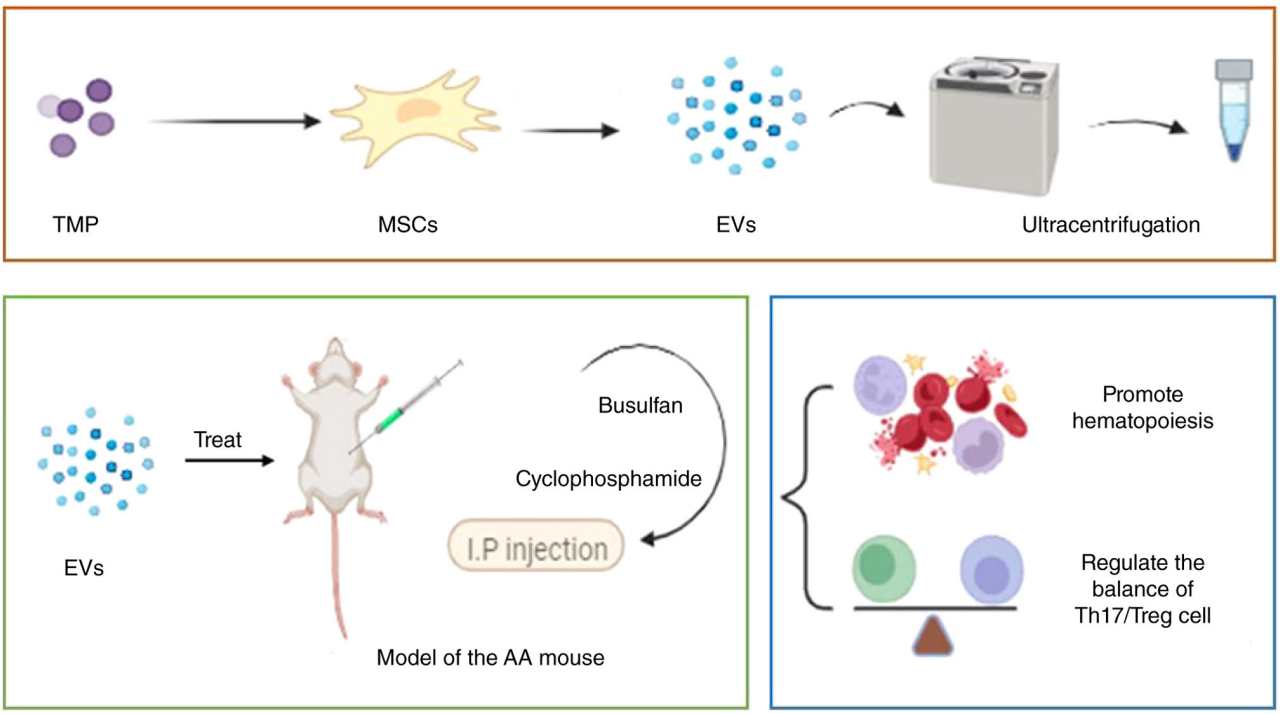


Figure 5. Schematic diagram depicting the workflow for generating TMP-stimulated MSCs-derived EVs and their therapeutic actions in AA mice. TMP pretreatment promotes EVs release from MSCs, and EVs are harvested by ultracentrifugation. The AA mouse model is induced by intraperitoneal administration of cyclophosphamide and busulfan. Treatment with these EVs improves hematopoiesis and modulates the Th17/Treg cell balance in AA mice. TMP, tetramethylpyrazine; AA, aplastic anemia; EVs, extracellular vesicles; MSCs, mesenchymal stem cells; Th17, T helper 17 cells; Tregs, regulatory T cells.

mice; however, the present study did not conduct functional hematopoietic colony-forming assays (such as CFU-GM), which is a limitation. Furthermore, the reduced spleen index and disrupted Th17/Treg cell balance in AA mice were restored by NC-EVs and TMP-EVs treatment, supporting the immunomodulatory effects of MSCs-EVs. Notably, NC-EVs and TMP-EVs produced comparable therapeutic effects in AA mice. Although TMP-EVs showed a greater therapeutic trend for some parameters, the differences were not statistically significant. These findings suggest that TMP primarily enhances MSCs-EVs secretion and may not substantially alter EVs cargo composition or biological activity. Further cargo profiling, including micro RNA (miRNA) and proteomic analyses, is required to confirm this possibility.

Various preconditioning approaches, including hypoxic culture, IFN-γ stimulation and TMP treatment, have been reported to promote EVs secretion from MSCs (18,33,34). Accordingly, *in vitro* preconditioning is widely considered an effective strategy for increasing the yield of MSCs-derived EVs; however, the molecular mechanisms by which TMP promotes MSCs-EVs secretion remain incompletely understood. Rab27a, a small GTPase of the Rab family, is a key regulator of membrane trafficking and EVs release (35). Several studies have established an essential role for Rab27a in EVs secretion. Song *et al* (36) demonstrated that stabilization of the Rab27a protein effectively enhanced EVs secretion. By contrast, Xu *et al* (37) reported that foot-and-mouth disease virus inhibited exosome secretion by inducing Rab27a degradation. Mechanistically, Rab27a deficiency prevents the docking of multivesicular endosomes with the plasma membrane, thereby suppressing EVs secretion (38). Consistent with these findings, the present results showed that TMP treatment markedly increased EVs particle abundance and the levels of the canonical EVs markers CD9 and CD63 in MSCs culture supernatants. TMP treatment also significantly upregulated Rab27a protein expression in MSCs, suggesting that Rab27a may be involved in TMP-induced MSCs-EVs secretion.

In addition to Rab27a signaling, mTORC1 is an important upstream regulator of EVs biogenesis and secretion. A previous study has shown that mTORC1 inhibition substantially promotes EVs release without markedly altering the overall protein and miRNA profiles of EVs (39). Moreover, mTORC1 suppression promotes the secretion of EVs enriched in senescence-associated factors, thereby delaying cellular senescence (40). As a central sensor of nutrients and growth signals, mTORC1 dynamically regulates EVs secretion in response to changes in the extracellular microenvironment (41). Emerging evidence also supports a functional interaction between mTORC1 and Rab27a. Zou *et al* (41) showed that Rab27a knockdown completely abolished rapamycin-induced EVs secretion, indicating that mTORC1 negatively regulates EVs release in a Rab27a-dependent manner. Consistent with these findings, the present dose-response experiments showed that TMP treatment increased Rab27a protein expression while decreasing mTORC1 levels in MSCs in a dose-dependent manner. Collectively, these results suggest that the Rab27a/mTORC1 signaling axis is associated with TMP-mediated MSCs-EVs secretion; however, the present study establishes only a preliminary correlative relationship within this regulatory pathway. Future studies using gene knockout and pharmacological inhibitor rescue experiments are needed to clarify the causal mechanism and regulatory

hierarchy of the Rab27a/mTORC1 axis in TMP-induced EVs secretion.

Nevertheless, the present study has several limitations. First, the cargo profiles of TMP-induced EVs, including their miRNA and functional protein contents, were not characterized. Second, the mechanistic findings were correlative, and causal validation using gene knockout or pharmacological rescue experiments was not performed. Third, only a single therapeutic dose was evaluated *in vivo*, and multidose validation in animal models is lacking. Moreover, EVs biodistribution analysis or systematic long-term safety assessment were not performed. Further studies incorporating long-term survival analyses and sustained monitoring of hematopoietic recovery are needed to comprehensively assess the safety and dose-dependent efficacy of intravenously administered EVs. Fourth, large-scale EVs production and good manufacturing practice-compliant preparation protocols remain insufficiently investigated, limiting the clinical translation of this therapeutic approach. Future studies should address these limitations to further evaluate the clinical potential of TMP-preconditioned MSCs-EVs for the treatment of AA.

In conclusion, the present study demonstrated that TMP promotes EV secretion from MSCs, potentially through modulation of the Rab27a/mTORC1 signaling axis. In addition, experimental evidence that EVs derived from TMP-preconditioned MSCs ameliorate BM failure and delay AA progression was provided (Fig. 5). These findings suggest that TMP-mediated enhancement of MSCs-EVs production may represent a feasible therapeutic approach for AA.

Acknowledgements

Not applicable.

Funding

The present study was supported by the 2022 Shenzhen Municipal Science and Technology Research Project of Shenzhen Municipal Science and Technology Innovation Committee (grant no. JCYJ20220530151613030), 2022 Health Science & Technology Project of Shenzhen Municipal Nanshan District Public Health Bureau (grant no. NS2022004), National Natural Science Foundation of China (grant no. 82474238), the National Natural Science Foundation of China (grant no. 82405133) and the Guangdong Basic and Applied Basic Research Foundation (grant no. 2024A1515010059).

Availability of data and materials

The data generated in the present study may be requested from the corresponding author.

Authors' contributions

LC and PD conducted the experiments. LC designed the experiments and wrote the paper. Data statistics and analysis were completed by XZ and FD. LK and XS contributed to data acquisition and critical revision of the manuscript. YX, JZ and ZL were mainly responsible for project design, critical revision of the manuscript for important intellectual content, and the acquisition of financial support. All authors read and approved the final version of the manuscript. LC and JZ confirm the authenticity of all the raw data.

Ethics approval and consent to participate

The animal experiment was approved by the Institutional Animal Care and Use Committee of Southern Medical University (approval no. SMUL2022228), in accordance with the ARRIVE guidelines. Human umbilical cords were collected after obtaining written informed consents and it was conducted in accordance with the guidelines for conducting clinical trials on human participants and the Declaration of Helsinki. This study protocol has been approved by the Ethics Committee of Shenzhen Qianhai Shekou Free Trade Zone Hospital (approval no. 2023-051-01).

Patient consent for publication

Not applicable.

Competing interests

The authors declare that they have no competing interests.

References

1. Scheinberg P: Acquired severe aplastic anaemia: how medical therapy evolved in the 20th and 21st centuries. Br J Haematol 194: 954-969, 2021.
2. Hosokawa K, Kajigaya S, Feng X, Desierto MJ, Fernandez Ibanez MD, Rios O, Weinstein B, Scheinberg P, Townsley DM and Young NS: A plasma microRNA signature as a biomarker for acquired aplastic anemia. Haematologica 102: 69-78, 2017.
3. Giudice V, Banaszak LG, Gutierrez-Rodrigues F, Kajigaya S, Panjwani R, Ibanez MDPF, Rios O, Bleck CK, Stempinski ES, Raffo DQ, *et al*: Circulating exosomal microRNAs in acquired aplastic anemia and myelodysplastic syndromes. Haematologica 103: 1150-1159, 2018.
4. Peslak SA, Olson T and Babushok DV: Diagnosis and treatment of aplastic anemia. Curr Treat Options Oncol 18: 70, 2017.
5. Chao YH, Wu HP, Chan CK, Tsai C, Peng CT and Wu KH: Umbilical cord-derived mesenchymal stem cells for hematopoietic stem cell transplantation. J Biomed Biotechnol 2012: 759503, 2012.
6. Fouillard L, Bensidhoum M, Bories D, Bonte H, Lopez H, Moseley AM, Smith A, Lesage S, Beaujean F, Thierry D, *et al*: Engraftment of allogeneic mesenchymal stem cells in the bone marrow of a patient with severe idiopathic aplastic anemia improves stroma. Leukemia 17: 474-476, 2003.
7. Clé DV, Santana-Lemos B, Tellechea MF, Prata KL, Orellana MD, Covas DT and Calado RT: Intravenous infusion of allogeneic mesenchymal stromal cells in refractory or relapsed aplastic anemia. Cytotherapy 17: 1696-1705, 2015.
8. Jaganathan BG, Tisato V, Vulliamy T, Dokal I, Marsh J, Dazzi F and Bonnet D: Effects of MSC co-injection on the reconstitution of aplastic anemia patient following hematopoietic stem cell transplantation. Leukemia 24: 1791-1795, 2010.
9. Xiao Y, Jiang ZJ, Pang Y, Li L, Gao Y, Xiao HW, Li YH, Zhang H and Liu Q: Efficacy and safety of mesenchymal stromal cell treatment from related donors for patients with refractory aplastic anemia. Cytotherapy 15: 760-766, 2013.
10. Weiss ARR and Dahlke MH: Immunomodulation by mesenchymal stem cells (MSCs): Mechanisms of action of living, apoptotic, and dead MSCs. Front Immunol 10: 1191, 2019.
11. Phelps J, Sanati-Nezhad A, Ungrin M, Duncan NA and Sen A: Bioprocessing of mesenchymal stem cells and their derivatives: Toward cell-free therapeutics. Stem Cells Int 2018: 9415367, 2018.

12. Baldari S, Di Rocco G, Piccoli M, Pozzobon M, Muraca M and Toietta G: Challenges and strategies for improving the regenerative effects of mesenchymal stromal cell-based therapies. Int J Mol Sci 18: 2087, 2017.
13. Eleuteri S and Fierabracci A: Insights into the secretome of mesenchymal stem cells and its potential applications. Int J Mol Sci 20: 4597, 2019.
14. Harting MT, Srivastava AK, Zhaorigetu S, Bair H, Prabhakara KS, Toledano Furman NE, Vykoukal JV, Ruppert KA, Cox CS Jr and Olson SD: Inflammation-Stimulated mesenchymal stromal cell-derived extracellular vesicles attenuate inflammation. Stem Cells 36: 79-90, 2018.
15. Sun Y, Shi H, Yin S, Ji C, Zhang X, Zhang B, Wu P, Shi Y, Mao F, Yan Y, *et al*: Human mesenchymal stem cell derived exosomes alleviate type 2 diabetes mellitus by reversing peripheral insulin resistance and relieving β-cell destruction. ACS Nano 12: 7613-7628, 2018.
16. Li X, Liu L, Yang J, Yu Y, Chai J, Wang L, Ma L and Yin H: Exosome derived from human umbilical cord mesenchymal stem cell mediates MiR-181c attenuating burn-induced excessive inflammation. EBioMedicine 8: 72-82, 2016.
17. Yang M, Lin L, Sha C, Li T, Zhao D, Wei H, Chen Q, Liu Y, Chen X, Xu W, *et al*: Bone marrow mesenchymal stem cell-derived exosomal miR-144-5p improves rat ovarian function after chemotherapy-induced ovarian failure by targeting PTEN. Lab Invest 100: 342-352, 2020.
18. Ruan XF, Ju CW, Shen Y, Liu YT, Kim IM, Yu H, Weintraub N, Wang XL and Tang Y: Suxiao Jiuxin pill promotes exosome secretion from mouse cardiac mesenchymal stem cells in vitro. Acta Pharmacol Sin 39: 569-578, 2018.
19. Ruan XF, Li YJ, Ju CW, Shen Y, Lei W, Chen C, Li Y, Yu H, Liu YT, Kim IM, *et al*: Exosomes from Suxiao Jiuxin pill-treated cardiac mesenchymal stem cells decrease H3K27 demethylase UTX expression in mouse cardiomyocytes in vitro. Acta Pharmacol Sin 39: 579-586, 2018.
20. Chen H, Deng C, Meng Z, Zhu M, Yang R, Yuan J and Meng S: Combined catalpol and tetramethylpyrazine promote axonal plasticity in Alzheimer's disease by inducing astrocytes to secrete exosomes carrying CDK5 mRNA and regulating STAT3 phosphorylation. Mol Neurobiol 61: 10770-10791, 2024.
21. Song X, Dai J, Li H, Li Y, Hao W, Zhang Y, Zhang Y, Su L and Wei H: Anti-aging effects exerted by Tetramethylpyrazine enhances self-renewal and neuronal differentiation of rat bMSCs by suppressing NF-kB signaling. Biosci Rep 39: BSR20190761, 2019.
22. Zhang L, Wang X, Lu X, Ma Y, Xin X, Xu X, Wang S and Hou Y: Tetramethylpyrazine enhanced the therapeutic effects of human umbilical cord mesenchymal stem cells in experimental autoimmune encephalomyelitis mice through Nrf2/HO-1 signaling pathway. Stem Cell Res Ther 11: 186, 2020.
23. Dominici M, Le Blanc K, Mueller I, Slaper-Cortenbach I, Marini F, Krause D, Deans R, Keating A, Prockop Dj and Horwitz E: Minimal criteria for defining multipotent mesenchymal stromal cells. The International Society for Cellular Therapy position statement. Cytotherapy 8: 315-317, 2006.
24. Théry C, Witwer KW, Aikawa E, Alcaraz MJ, Anderson JD, Andriantsitohaina R, Antoniou A, Arab T, Archer F, Atkin-Smith GK, *et al*: Minimal information for studies of extracellular vesicles 2018 (MISEV2018): A position statement of the International Society for Extracellular Vesicles and update of the MISEV2014 guidelines. J Extracell Vesicles 7: 1535750, 2018.
25. Young NS: Aplastic anemia. N Engl J Med 379: 1643-1656, 2018.
26. Guillamat-Prats R: The role of MSC in wound healing, scarring and regeneration. Cells 10: 1729, 2021.
27. Lai RC, Yeo RW and Lim SK: Mesenchymal stem cell exosomes. Semin Cell Dev Biol 40: 82-88, 2015.
28. Thongsit A, Oontawee S, Siriarchavatana P, Rodprasert W, Somparn P, Na Nan D, Osathanon T, Egusa H and Sawangmake C: Scalable production of anti-inflammatory exosomes from three-dimensional cultures of canine adipose-derived mesenchymal stem cells: Production, stability, bioactivity, and safety assessment. BMC Vet Res 21: 81, 2025.
29. Muok L, Sun L, Esmonde C, Worden H, Vied C, Duke L, Ma S, Zeng O, Driscoll T, Jung S and Li Y: Extracellular vesicle biogenesis of three-dimensional human pluripotent stem cells in a novel Vertical-Wheel bioreactor. J Extracell Biol 3: e133, 2024.
30. Lobb RJ, Becker M, Wen SW, Wong CS, Wiegmans AP, Leimgruber A and Möller A: Optimized exosome isolation protocol for cell culture supernatant and human plasma. J Extracell Vesicles 4: 27031, 2015.
31. Gao M, Cai J, Zitkovsky HS, Chen B and Guo L: Comparison of yield, purity, and functional properties of large-volume exosome isolation using ultrafiltration and polymer-based precipitation. Plast Reconstr Surg 149: 638-649, 2022.
32. Zhang X, Gao L, Hu X, Chen S, Nie L and Zhu L: Tetramethylpyrazine promotes bone marrow repair in a C57 mouse model of X-rayinduced immune-mediated bone marrow failure. Nan Fang Yi Ke Da Xue Xue Bao 39: 957-963, 2019 (In Chinese).
33. Ren L, Song ZJ, Cai QW, Chen RX, Zou Y, Fu Q and Ma YY: Adipose mesenchymal stem cell-derived exosomes ameliorate hypoxia/serum deprivation-induced osteocyte apoptosis and osteocyte-mediated osteoclastogenesis in vitro. Biochem Biophys Res Commun 508: 138-144, 2019.
34. Zhang G, Zhu Z, Wang H, Yu Y, Chen W, Waqas A, Wang Y and Chen L: Exosomes derived from human neural stem cells stimulated by interferon gamma improve therapeutic ability in ischemic stroke model. J Adv Res 24: 435-445, 2020.
35. Kimura T and Niki I: Rab27a in pancreatic beta-cells, a busy protein in membrane trafficking. Prog Biophys Mol Biol 107: 219-223, 2011.
36. Song L, Tang S, Han X, Jiang Z, Dong L, Liu C, Liang X, Dong J, Qiu C, Wang Y and Du Y: KIBRA controls exosome secretion via inhibiting the proteasomal degradation of Rab27a. Nat Commun 10: 1639, 2019.
37. Xu G, Xu S, Shi X, Shen C, Zhang D, Zhang T, Hou J, Zhang K, Zheng H and Liu X: Foot-and-mouth disease virus degrades Rab27a to suppress the exosome-mediated antiviral immune response. Vet Microbiol 251: 108889, 2020.
38. Sinha S, Hoshino D, Hong NH, Kirkbride KC, Grega-Larson NE, Seiki M, Tyska MJ and Weaver AM: Cortactin promotes exosome secretion by controlling branched actin dynamics. J Cell Biol 214: 197-213, 2016.
39. Luo X, Feng W, Huang S, Miao S, Jiang T, Lei Q, Yin J, Zhang S, Bai X, Hao C, *et al*: Odontoblasts release exosomes to regulate the odontoblastic differentiation of dental pulp stem cells. Stem Cell Res Ther 14: 176, 2023.
40. Zou W, Lai M, Jiang Y, Mao L, Zhou W, Zhang S, Lai P, Guo B, Wei T, Nie C, *et al*: Exosome release delays senescence by disposing of obsolete biomolecules. Adv Sci (Weinh) 10: e2204826, 2023.
41. Zou W, Lai M, Zhang Y, Zheng L, Xing Z, Li T, Zou Z, Song Q, Zhao X, Xia L, *et al*: Exosome release is regulated by mTORC1. Adv Sci (Weinh) 6: 1801313, 2018.

Copyright © 2026 Chen et al. This work is licensed under a Creative Commons Attribution-NonCommercial-NoDerivatives 4.0 International (CC BY-NC-ND 4.0) License.